Theor Chem Acc (2009) 124:251–259
DOI 10.1007/s00214-009-0605-1

REGULAR ARTICLE

A multiconfigurational perturbation theory study of the electronic structure and EPR *g* values of an oxomolybdenum enzyme model complex

Steven Vancoillie · Kristine Pierloot

Received: 31 March 2009 / Accepted: 9 July 2009 / Published online: 24 July 2009

Abstract We have studied the electronic structure (ground and excited states) and **g** matrix of a model compound for oxomolybdenum enzymes featuring the MoO–dithiolate moiety in C_s symmetry, by means of multiconfigurational second-order perturbation theory (CASPT2) for a range of fold angles (5–29°), i.e. the angle between the S–Mo–S and S–C–C–S planes of the dithiolate ligand. We found no evidence of a suggested 3-center pseudo-σ bonding interaction between the singly occupied orbital of the ground state and the symmetric in-plane dithiolate orbital (Inscore et al. in Inorg Chem 38:1401–1410, 1999). This is complemented with our alternative assignment of band **4** in the electronic spectrum as the transition out of the a″ instead of the a′ dithiolate in-plane orbital into the singly occupied ground-state orbital, believed to probe the dominant hole superexchange pathway (Inscore et al. in Inorg Chem 38:1401–1410, 1999; Burgmayer et al. in J Inorg Biochem 101:1601–1616, 2007). Principal *g* values of 1.9652, 1.9090, 2.0003 were obtained at a fold angle of 21°. The latter value is so close to the free electron g_e factor is due to an important positive contribution from the LMCT transition corresponding to band **4**, counteracting the negative contributions from the ligand field transitions.

Keywords Multiconfigurational methods · Electronic structure · EPR · Molybdenum enzymes

S. Vancoillie (✉) · K. Pierloot
K.U.Leuven, Celestijnenlaan 200F,
3001 Heverlee, Belgium
e-mail: steven.vancoillie@chem.kuleuven.be

1 Introduction

Molybdenum plays an important role in biology as the catalytic center of a broad range of enzymes involved in the nitrogen, sulfur and carbon metabolism [3] as well as in the more exotic arsenic, selenium and chlorine metabolism [4]. The vast majority of these enzymes contains a terminal oxygen ligand associated with the molybdenum active center, and they are often referred to as oxomolybdenum enzymes.

All of these mononuclear molybdenum enzymes possess at least one pterin cofactor, termed "molybdopterin" or "pyranopterin" [3], which binds to the molybdenum core via a dithiolate group. The fact that pyranopterin is an integral part of the active site strongly points to an active role in the catalytic process, by acting as an electronic buffer during electron transfer reactions [5] providing an orbital pathway for electron transfer regeneration of the active site [1] and by modulating the reduction potential of the active site [1, 3, 6, 7].

The in situ study of the electronic structure of the active site of molybdenum enzymes by electronic absorption spectroscopy is not possible, due to the presence of additional prosthetic groups (hemes, iron sulfur centers, flavins) with overlapping intense electronic absorptions [8]. In contrast, magnetic circular dichroism (MCD) and electron paramagnetic resonance (EPR) spectroscopy can provide valuable information on the paramagnetic Mo(V) center, not hampered by the surrounding diamagnetic chromophores. Nevertheless, the study of representative well-characterized Mo(V) complexes is still an important prerequisite for a detailed understanding of the MCD spectra of molybdenum enzymes. A whole range of model systems have been synthesized and studied in detail by electronic absorption, MCD, and EPR spectroscopy [1, 2, 6–14].

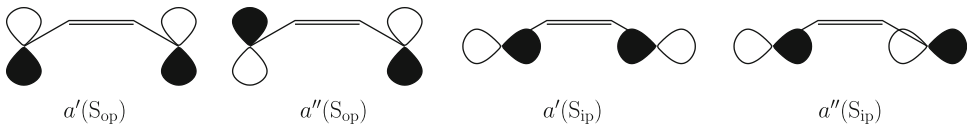

Fig. 1 Schematic plot of the highest occupied MOs of the dithiolate ligand

Of particular importance is the class of LMoO(S–S) type compounds, where S–S is a dithiolate ligand which forms a five-membered ring with Mo(V). These complexes possess C_s symmetry, with a strong axial Mo–O bond along the z axis, and the thiolate sulfur atoms mirrored by the σ_{yz} mirror plane. The four dithiolate frontier orbitals involved in the bonding with Mo are schematically presented in Fig. 1. The two S_{op} orbitals are oriented perpendicular to the dithiolate plane, while the two S_{ip} orbitals are oriented within this plane. The $a''(S_{ip})$ orbital is involved in covalent σ bonding with molybdenum. It has also been suggested that the $a'(S_{ip})$ orbital might be involved in a three-center σ bond with molybdenum, thereby providing an efficient in-plane electron transfer pathway [15].

An important feature emerging from each of the previous studies of the LMoO(S–S) models is the dithiolate fold angle, this is the angle between the S–Mo–S and S–C–C–S plane (Fig. 2). The fold angle is suggested to modulate the electronic structure of the active site through electron donation from the $a'(S_{op})$ orbital to molybdenum and is sensitive to the overall electronic structure of the dithiolate [16–18]. The energy barrier for varying the fold angle in Mo(V)–dithiolate complexes has been shown to be very low: of the order of 1 kcal mol^{-1} over a range of more than 30° [19].

Most of the studies cited above used computational methods to aid in the investigation of the electronic structure of the dithiolate complexes. These studies were, however, limited to calculations on the ground state by means of density functional theory (DFT). In this work we present a computational study of the electronic structure of the ground state, the EPR **g**-matrix as well as the electronic absorption spectrum by means of multi-state second-order perturbation theory based on a multiconfigurational reference wavefunction, i.e. CASSCF/MS-CASPT2.

We have chosen (Tp*)MoO(bdt) as a model complex (Fig. 3), with Tp* = hydrotris(3,5-dimethyl-1-pyrazolyl)borate and bdt = benzenedithiolate, because of the availability of an extensive analysis of the electronic absorption spectrum in Ref. [1], where the six lowest energy bands (up to 25,000 cm^{-1}) of the spectrum have been assigned with the help of MCD and Resonance Raman spectroscopy. Furthermore, a recent density functional study is available of the electronic structure and spin hamiltonian parameters (**g**-matrix, ^{95}Mo hyperfine matrix) of this compound [20]. This study also touched the issue of the fold angle, experimental versus DFT optimized, pointing to the need of studying the fold-angle dependence

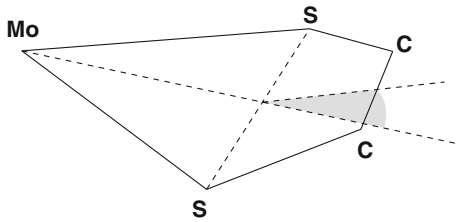

Fig. 2 Schematic plot of the dithiolate fold angle (*grey*)

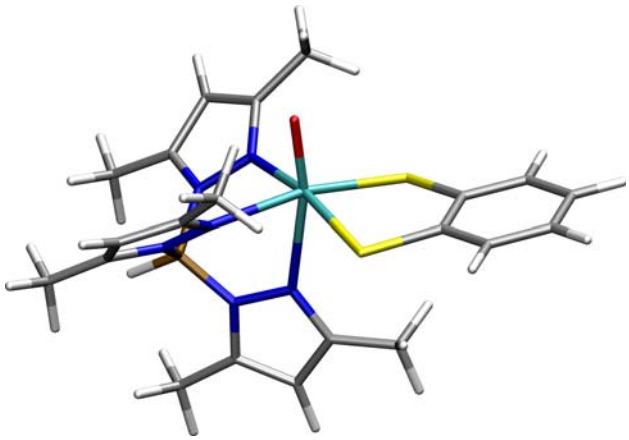

Fig. 3 Stick representation of the (Tp*)MoO(bdt) molecule

of the g-matrix. Therefore, we have decided to study a range of fold angles between 5° and 29°. A preliminary study on a truncated (Tp*)MoO(bdt) model, using smaller basis sets and single-state CASPT2, was previously reported by us [21]. No fold angle variation in the structure was taken into account, instead the B3LYP DFT optimum was used. To the best of our knowledge, this is the first ab initio computational study of the **g**-matrix of a (Tp*)MoO(S–S) type model compound.

2 Computational details

The structure of (Tp*)MoO(bdt) was optimized by means of DFT within the C_s point group. To study the influence of the fold angle (angle between S–Mo–S and S–C=C–S plane) on the ground-state energy, the electronic absorption spectrum, and the **g**-matrix at the CASPT2 level, a number of DFT optimizations with a fixed fold angle, ranging from 5° to 29° with 4° intervals, were performed. These calculations were performed with TURBOMOLE V5.9 [22], using the PBE0 functional [23–27]. TZVP basis sets were used

for all atoms except molybdenum, the 18 electron core of which was described by a relativistic ECP and the valence region by a TZVP basis set [28, 29]. For the subsequent single-point calculations and the description of the electronic spectrum, the molecule was oriented with the Mo–O bond along the positive z axis and with the yz-plane as the mirror plane.

To study the electronic structure of the ground and excited states, CASSCF [30]/CASPT2 [31, 32] single-point calculations were performed at each of the DFT optimized geometries, making use of the MOLCAS 7.0 code [33]. Scalar relativistic effects were included using a Douglas–Kroll–Hess (DKH) Hamiltonian [34–36]. In all CASPT2 calculations the core electrons were kept frozen, except for the Mo 4s, 4p orbitals. To avoid intruder states and to give a balanced description of open and closed-shell systems, an imaginary level shift of 0.1 and an (standard) IPEA shift of 0.25 were used [37, 38]. ANO-rcc basis sets were used for the central metal atom and the directly bonded ligand atoms with the following contractions: Mo [8s7p5d2f1g]; S [5s4p2d]; O, N [4s3p1d]. For all other atoms, ANO-s basis sets were used with the following contractions: C (bdt), B, N [3s2p1d]; C (Tp*) [3s2p]; H (bdt, B) [2s1p]; H (Tp*) [2s]. The recent addition of the Cholesky decomposition of the matrix of the two-electron repulsion integrals in the MOLCAS 7.0 package was used (treshold of $10^{-6}E_h$) [39].

Two different active spaces were used for the CASSCF/CASPT2 calculations. Active space CAS(9in9) is built from distributing 9 electrons among the five molybdenum 4d orbitals, the three oxygen 2p orbitals, and the dithiolate $a''(S_{ip})$ orbital (which also contains a small contribution from the nitrogen-bonded ligand). The latter four orbitals constitute the bonding combinations corresponding to the antibonding σ and π-type molybdenum 4d orbitals. They are included to describe nondynamical correlation effects associated with covalent metal–ligand interactions [40, 41]. In CAS(15in12), three extra dithiolate orbitals ($a'(S_{ip})$, $a'(S_{op})$ and $a''(S_{op})$) were included to allow for the calculation of all possible sulfur-to-metal charge-transfer states within the considered energy range.

The optimum fold angle at the CASPT2 level was determined by a series of ground-state calculations on the different DFT structures with the CAS(9in9) space. For all structures, state-average MS-CASPT2 calculations were performed with the CAS(15in12) active space, including eight and ten states for the A′ and A″ irreducible representations respectively. Oscillator strengths were obtained using the RASSI method [42]. The number of excited states included in each irreducible representation was based on two requirements. First of all we want to include the entire experimental absorption spectrum (below 34,000 cm^{-1}). Secondly, for the calculation of the g factors we need to include all important ligand-field and charge-transfer states [43, 44]. The calculations of the **g** matrix were performed by treating the Zeeman effect through first-order degenerate perturbation theory within the lowest Kramers doublet [44, 45]. This method is implemented in the MOLCAS RASSI code, making use of perturbation-modified CASSCF (PMCAS) wavefunctions and MS-CASPT2 energies [46], treating spin-orbit coupling through the atomic mean-field integral (AMFI) approximation [47–49].

3 Results and discussion

3.1 Geometry

(Tp*)MoO(bdt) consists of a Mo(V) ion surrounded by three ligands in a pseudo-octahedral arrangement: a strongly (triple) bound axial O^{2-} atom, bdt equatorially bonded via two sulfur atoms, and Tp* bonded to molybdenum through two equatorial nitrogen atoms and one weakly coordinated axial nitrogen atom. The DFT structures of (Tp*)MoO(bdt) with fold angles of 5° and 29° are shown in Fig. 4. As the figure shows, the bond distances between Mo and its direct neighbours hardly vary between these two angles. The PBE0-DFT and CASPT2 energies as a function of the fold angle are shown in Fig. 5. The potential energy surface is extremely flat with respect to the variation of the fold angle. Between 5° and 29°, the DFT energies vary with 0.81 kcal mol^{-1}, and the CASPT2 energies by at most 0.35 kcal mol^{-1}. Because of this, the fold angle can be expected to be strongly influenced by the crystal structure (model species) or the protein environment (molybdenum enzymes). The experimental fold angle of (Tp*)MoO(bdt), obtained from X-ray crystallography, is 21.3° [9, 10]. As the energy required for changing the fold angle is very low (<1 kcal mol^{-1}), direct comparison between the experimental X-ray (solid) and the calculated DFT and CASPT2 (vacuum) fold angle is rather

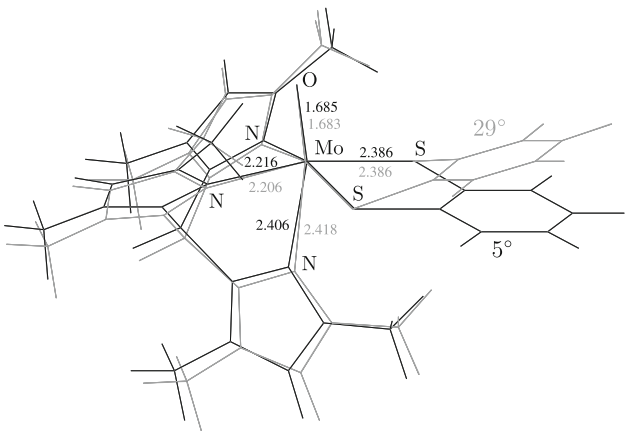

Fig. 4 Optimized geometry of (Tp*)MoO(bdt)

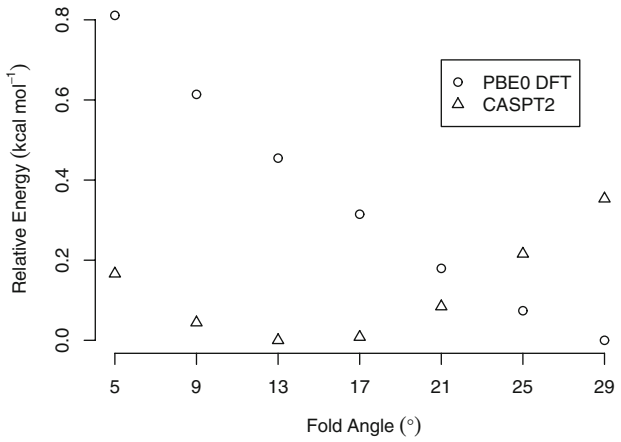

Fig. 5 Potential energy surface DFT/CASPT2

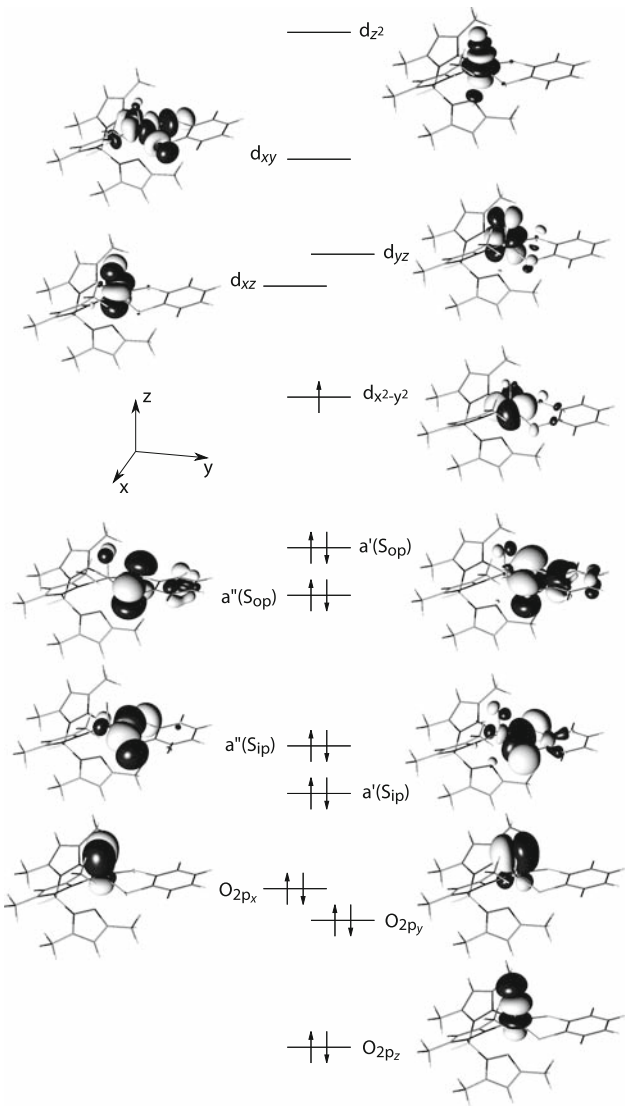

Fig. 6 Natural orbitals constituting the active space

meaningless. When comparing the calculated values, we note that the fold angle obtained from DFT, 30.8°, is much larger than the angle obtained from CASPT2, 14.4°.

3.2 Electronic structure and spectrum

The pseudo-octahedral arrangement of the ligands surrounding the formal Mo(V) in (Tp*)MoO(bdt) gives rise to a splitting of the *d* orbitals dominated by the strongly covalent molybdenum-oxygen triple bond. A schematic overview of the orbitals and their energies is given in Fig. 6. σ interaction between the Mo $4d_{z^2}$ and the O $2p_z$ orbital, and π interaction between the Mo $4d_{xz,yz}$ and the O $2p_{x,y}$ orbitals give rise to bonding–antibonding pairs of molecular orbitals, resulting in a strong destabilization of the antibonding, primarily metal-based combinations. The Mo $4d_{xy}$ orbital is destabilized by σ interactions with the N and (primarily) S atoms of the equatorial ligands. The deviation from octahedral symmetry is most apparent in the latter interaction, since the bonding σ interaction is strongly directed towards the dithiolate ligand, as can be seen in the picture of the $a''(S_{ip})$ orbital (Fig. 6). The non-interacting Mo $4d_{x^2-y^2}$ orbital is least destabilized, thus becoming the singly occupied molecular orbital (SOMO) in the Mo(V) ground state.

A closer look at the $a'(S_{op})$ orbital shows that it has a small contribution from Mo $d_{x^2-y^2}$. It has been proposed that anisotropic covalency contributions involving the out-of-plane orbitals of the ditholene ligand control the molybdenum reduction potential by modulating the effective charge on the metal [1, 7, 13, 15]. It has been suggested that this modulation is regulated through the dithiolate fold angle. Folding the ditholate plane upwards in the direction of the Mo–O bond leads to an increased overlap between the $a'(S_{op})$ and the Mo $d_{x^2-y^2}$ orbitals, thus giving rise to a reduced effective charge on the metal. However, according to our calculations, the effective charge of the molybdenum atom (obtained from a Mulliken population analysis of the ground state), shows only a very small increase from +0.89 to +0.91 *e* as the fold angle changes from 5° to 29°, thus not supporting the charge modulating role of the dithiolate fold angle.

Since the variation of the Mo(V)–dithiolate fold angle has further been indicated as a key factor in the ability of the pterin ring to tune the electron density at the active site of molybdenum enzymes [16, 17] we decided to include the fold-angle dependence of the electronic spectrum and g-factors from the start, rather than to calculate these properties only for one specific fold angle. For each of the DFT structures with fold angles ranging from 5° to 29°, the excitation energy, composition and oscillator strength of the excited states of A′ and A″ symmetry are presented in Fig. 7.

Two types of excitations make up the calculated electronic spectrum. First, there are three LF excitations from

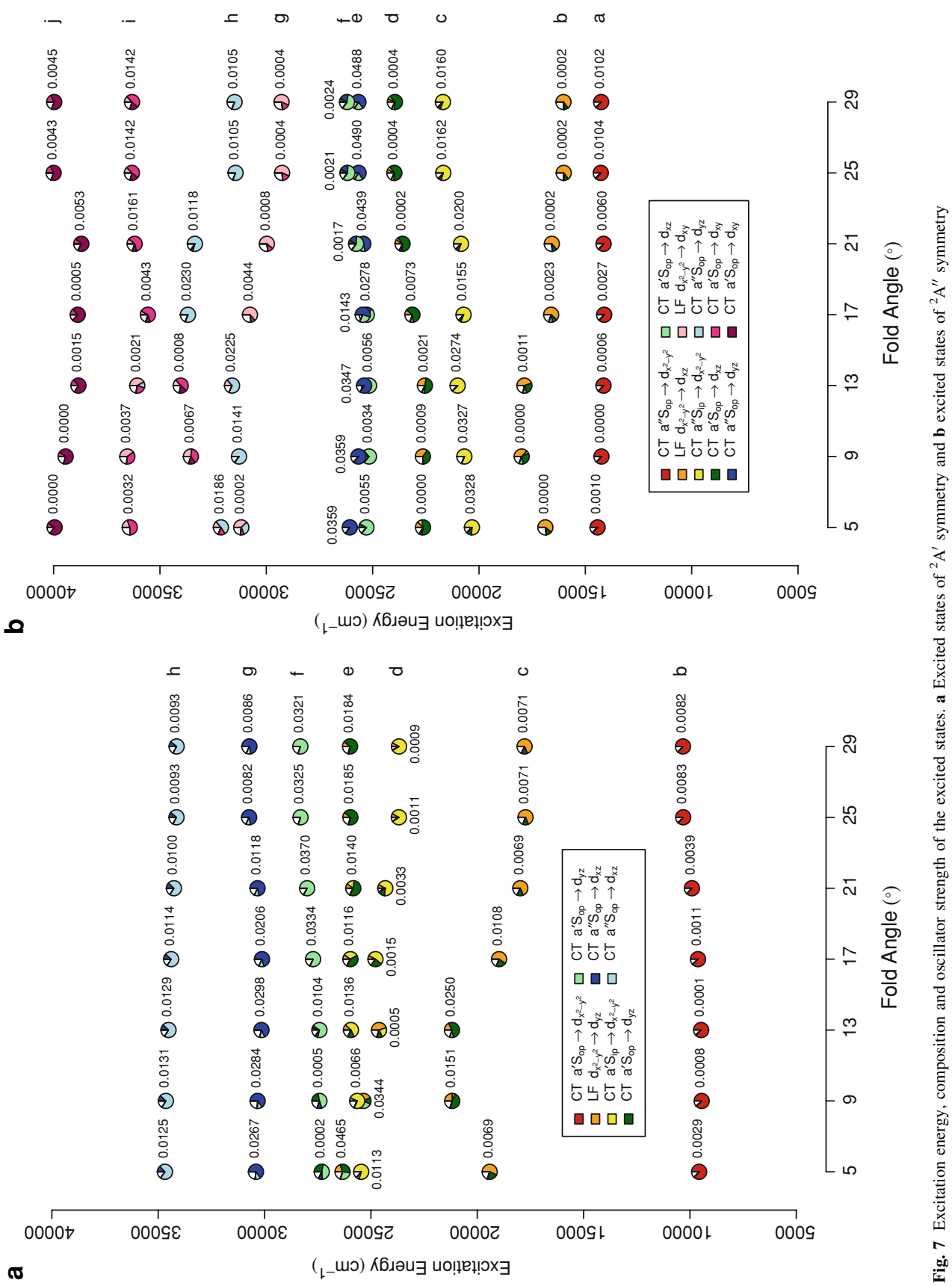

Fig. 7 Excitation energy, composition and oscillator strength of the excited states. **a** Excited states of $^2A'$ symmetry and **b** excited states of $^2A''$ symmetry

Mo $d_{x^2-y^2}$ into the Mo d_{xz}, d_{yz} and d_{xy} orbitals. The Mo d_{z^2} orbital is so strongly destabilized by σ interaction with the oxygen atom, that excitations into this orbital transition are absent from the calculated spectrum. The second type are the LMCT excitations out of the highest four occupied dithiolate orbitals. We can distinguish two groups of LMCT excitations. Excitations out of the S_{op} and S_{ip} orbitals into Mo $d_{x^2-y^2}$ (ground-state SOMO) give rise to four LMCT states characterized by one unpaired electron in each of these dithiolate orbitals. Excitations out of the $a'(S_{op})$ orbital into the Mo d_{xz}, d_{yz} and d_{xy} orbitals, and out of the $a''(S_{op})$ orbital into the Mo d_{xz} and d_{yz} orbitals give rise to respectively three and two pairs of doublets, characterized by three unpaired electrons. Together with the ground state, this makes a total of eighteen states, of which eight belong to the A′ irrep (Fig. 7a) and ten belong to the A″ irrep (Fig. 7b).

The part of the electronic absorption spectrum below 15,000 cm^{-1} is exclusively built from the two LMCT transitions out of the S_{op} orbitals into the Mo $d_{x^2-y^2}$ ground-state SOMO (red) at approximately 10,000 cm^{-1} ($b^2A' : a'(S_{op}) \rightarrow d_{x^2-y^2}$) and 15,000 cm^{-1} ($a^2A'' : a''(S_{op}) \rightarrow d_{x^2-y^2}$). These two states do not show any significant mixing with other excitation types and their excitation energy remains constant over the entire range of fold angles. The oscillator strength of both states generally increases towards larger fold angles.

The second excited state of each symmetry corresponds to a LF transition from the Mo $d_{x^2-y^2}$ SOMO into the Mo d_{yz} (c^2A' at 18,000 cm^{-1}) and d_{xz} (b^2A'' at 16,000 cm^{-1}) orbitals (orange). The LMCT excitations out of the $a'(S_{op})$ orbital into the latter two orbtals at 26,000 cm^{-1} (e^2A') and 24,000 cm^{-1} (d^2A'') (dark green) show significant mixing with these LF transitions at lower fold angles. This leads to an increase in energy of both states. Only for the c^2A' LF state does this also lead to an increase in oscillator strenght, which is borrowed from the e^2A' LMCT state.

The next two excited states (yellow) are LMCT transitions corresponding to an excitation of an electron out of the two S_{ip} orbitals into Mo $d_{x^2-y^2}$. They occur around 24,000–25,000 cm^{-1} (d^2A') and 20,000–22,000 cm^{-1} (c^2A''). The excitation energy of the d^2A' state decreases towards higher fold angles, while that of the c^2A'' state increases. The oscillator strength of the c^2A'' state is much higher than that of the d^2A' state, both decreasing with respect to higher fold angles.

Excitations out of the S_{op} orbitals into Mo d_{yz}, d_{xz} are situated in the region between 25,000 and 35,000 cm^{-1}. In general, within each symmetry, transitions out of $a'(S_{op})$ (green) are at lower energies than transitions out of $a''(S_{op})$ (blue). The oscillator strenghts of the $S_{op} \rightarrow d_{xz}$ transitions decrease with an increasing fold angle, while the reverse is true for the $S_{op} \rightarrow d_{yz}$ transitions. The corresponding excitation energies are quite steady (variations of at most 2,000 cm^{-1} from left to right), except for some irregularities due to mixing with LF states.

The g^2A'' state at approximately 30,000 cm^{-1} can only be discriminated as the $a'(d_{x^2-y^2}) \rightarrow a''(d_{xy})$ LF transition at high angles. At low angles it is heavily mixed with the h^2A'' or i^2A'' state. The latter state belongs to the region >35,000 cm^{-1} containing the pair of doublet $S_{op} \rightarrow d_{xy}$ transitions of A″ symmetry.

Table 1 Band assignment of the electronic absorption spectrum at a fold angle of 21°

CASPT2 (15in12)			Experiment [1, 2, 8]	
State	ΔE (Osc. Str.)	Excitation composition	Band	ΔE (Osc. Str.)
X^2A'		82%$[d^1_{x^2-y^2}]$		
b^2A'	9,907 (0.0039)	87%$[a'(S_{op}) \rightarrow a'(d_{x^2-y^2})]$	**1**	9,100 (0.0056)
a^2A''	14,144 (0.0060)	87%$[a''(S_{op}) \rightarrow a'(d_{x^2-y^2})]$	**2**	13,100 (0.0033)
b^2A''	16,576 (0.0002)	64%$[a'(d_{x^2-y^2}) \rightarrow a''(d_{xz})]$		
		10%$[a'(S_{op}) \rightarrow a''(d_{xz})]^l$		
c^2A'	17,975 (0.0069)	69%$[a'(d_{x^2-y^2}) \rightarrow a'(d_{yz})]$	**3**	15,800 (−)
		13%$[a'(S_{op}) \rightarrow a'(d_{yz})]^l$		
c^2A''	20,845 (0.0200)	81%$[a''(S_{ip}) \rightarrow a'(d_{x^2-y^2})]$	**4**	19,400 (0.0160)
		6%$[a'(S_{op}) \rightarrow a''(d_{xz})]^l$		
d^2A''	23,594 (0.0002)	62%$[a'(S_{op}) \rightarrow a''(d_{xz})]^l$		
		9%$[a'(d_{x^2-y^2}) \rightarrow a''(d_{xz})]$		
		6%$[a''(S_{ip}) \rightarrow a'(d_{x^2-y^2})]$		
		5%$[a'(S_{op}) \rightarrow a''(d_{xz})]^h$		
d^2A'	24,325 (0.0033)	69%$[a'(S_{ip}) \rightarrow a'(d_{x^2-y^2})]$	**5**	22,100 (0.0170)
		15%$[a'(S_{op}) \rightarrow a'(d_{yz})]^l$		
e^2A''	25,438 (0.0439)	65%$[a''(S_{op}) \rightarrow a'(d_{yz})]^l$	**6**	25,100 (0.0920)
		20%$[a'(S_{op}) \rightarrow a''(d_{xz})]^h$		
f^2A''	25,774 (0.0017)	59%$[a'(S_{op}) \rightarrow a''(d_{xz})]^h$		
		18%$[a''(S_{op}) \rightarrow a'(d_{yz})]^l$		
		8%$[a'(S_{op}) \rightarrow a''(d_{xz})]^l$		
e^2A'	25,829 (0.0140)	56%$[a'(S_{op}) \rightarrow a'(d_{yz})]^l$		
		17%$[a'(S_{ip}) \rightarrow a'(d_{x^2-y^2})]$		
		10%$[a'(d_{x^2-y^2}) \rightarrow a'(d_{yz})]$		
f^2A'	27,999 (0.0370)	83%$[a'(S_{op}) \rightarrow a'(d_{yz})]^h$		
g^2A''	29,972 (0.0008)	61%$[a'(d_{x^2-y^2}) \rightarrow a''(d_{xy})]$		
		12%$[a'(S_{op}) \rightarrow a''(d_{xy})]^l$		

An extensive analysis of the experimental electronic absorption and MCD spectra of (Tp*)MoO(bdt) was performed by Inscore et al. in 1999, resulting in the assignment of six bands. In C_s symmetry, a positive MCD signal is observed for transitions involving a change in symmetry ($A' \leftarrow A''$) and a negative MCD signal is observed for transitions between states of the same symmetry ($A' \leftarrow A'$) [8]. In this work, we have based our assignment of the bands in the experimental spectrum on the fold angle closest to the one obtained from single-crystal X-ray crystallography (RT), i.e. 21°. For the latter structure, a detailed description of the composition of each state, together with the excitation energy and oscillator strength is given in Table 1. We will refer to the experimental bands with the same number as in Ref. [1].

Our calculations confirm the assignment of bands **1** and **2** at 9,100 and 13,100 cm^{-1} respectively as the LMCT transitions out of the $a', a''(S_{op})$ orbitals into the Mo $a'(d_{x^2-y^2})$ orbital. The energy ordering corresponds to the assignment of the (Tp*)Mo(S_2DIFPEPP) spectrum, the transition out of the $a'(S_{op})$ orbital being the lowest in energy [2]. The increase in oscillator strength of the latter transition towards larger fold angles could point to an increasing (though very small) overlap between the $a'(S_{op})$ and Mo $a'(d_{x^2-y^2})$ orbitals. Band **3** has previously been assigned as the $a'(d_{x^2-y^2}) \rightarrow a'(d_{yz}), a''(d_{xz})$ ligand field transitions, again conform with our calculations. Based on its oscillator strength and positive MCD signature, the $a'(d_{x^2-y^2}) \rightarrow a'(d_{yz})$ transition should be held responsible for the electronic absorption peak, even though the energy of the $a'(d_{x^2-y^2}) \rightarrow a''(d_{xz})$ transition is closer to the experimental band position. Despite this remaining uncertainty, there can be little or no doubt about the assignment of band **3** as a ligand field transition.

The first band where our calculations disagree with previous assignments is band **4** at 19,400 cm^{-1}. Originally, this band was assigned as a ligand field transition [8]. However, more recently, it was assigned as the $a'(S_{ip}) \rightarrow a'(d_{x^2-y^2})$ transition in Refs. [1, 2]. This was based on the relatively high intensity of this band, supposedly originating from a large overlap between the donor and acceptor orbital involved. To explain this large overlap, formation of a covalent three-centered pseudo σ bond between the $a'(S_{ip})$ and Mo $a'(d_{x^2-y^2})$ orbitals was suggested. Our calculations do not show any sign of the existence of such a bond. In fact, apart from the tiny covalent interaction with $a'(S_{op})$ orbital, the ground state singly occupied orbital is almost completely non-bonding. Together with the fact that the $a'(S_{ip}) \rightarrow a'(d_{x^2-y^2})$ excitation shows up at a much higher energy in the calculated electronic absorption spectrum than the energy of band **4**, we instead assign the latter as the $a''(S_{ip}) \rightarrow a'(d_{x^2-y^2})$ excitation, thus matching both the expected energy and intensity. As the $a''(S_{ip})$ orbital is involved in σ bonding with the Mo d_{xy} orbital, an excitation out of this orbital weakens the Mo–S bonds. Thus, our assignment still agrees with the observed resonance Raman enhancement of the in-plane vibrational modes within the envelope af band **4**, indicating an LMCT transition strongly localized in the dithiolate–Mo plane [1].

Based on its energy and oscillator strength, the state which is most likely responsible for band **5** is the fourth excited state within A′ symmetry (d^2A'). This state contains a mixture of $a'(S_{ip}) \rightarrow a'(d_{x^2-y^2})$ and $a'(S_{op}) \rightarrow a'(d_{yz})$ transitions, the latter of which could account for the resonance Raman enhancement of the Mo≡O stretching mode. In reality, this band is much more intense than the calculated oscillator strength suggests. We therefore believe that in reality the d^2A' state has a larger $a'(S_{op}) \rightarrow a'(d_{yz})$ contribution relative to $a'(S_{ip}) \rightarrow a'(d_{x^2-y^2})$, thus leading to an increased intensity borrowing from the e^2A' state.

Turning to band **6** there are three possible states within the correct energy range. Based on the intensity of the band, we assign this as an excitation to the e^2A'' state. The latter is a mixture of the $a''(S_{op}) \rightarrow a'(d_{yz})$ (65%) and the $a'(S_{op}) \rightarrow a''(d_{xz})$ (20%) transitions.

3.3 *g* Matrix

Before discussing the principal *g* values of (Tp*)MoO(bdt), we will give a short description of the *g* values of the more symmetric and simpler $MoOX_4^-$ (with X = halogen F, Cl, Br) series of complexes, which we have studied in detail in a previous paper [44]. This should provide a better picture of the various excited states involved in the contributions to the **g** matrix.

$MoOX_4^-$ is a molecule with C_{4v} symmetry, characterized by a strong Mo–O bond along the C_4 axis (*z* axis). The four halogen ligands are situated between the *x* and *y* axes. This gives rise to a ligand field splitting in which the d_{z^2} and d_{xy} orbitals are destabilized by covalent σ interaction with the oxygen and halogen ligands, and the d_{xz} and d_{yz} orbitals by π interaction with the oxygen atom, leaving the $d_{x^2-y^2}$ orbital as the singly occupied orbital in the ground state.

Within the choice of coordinate system, the **g** matrix of $MoOX_4^-$ is already diagonal giving rise to two equal in-plane g_{xx} and g_{yy} values ($g_\perp$) and one axial g_{zz} value ($g_\parallel$) along the *x*, *y* and *z* axis, respectively. The ligand field excitations out of the $d_{x^2-y^2}$ orbital into the $d_{xz,yz}$ and d_{xy} orbitals give a negative contribution to $g_\perp$ and $g_\parallel$ respectively. The ligand-to-metal charge transfer from the bonding d_{xy}–ligand combination into $d_{x^2-y^2}$ gives rise to a positive contribution to $g_\parallel$. The latter LMCT contribution increases as the σ-bonds between the halogens and Mo $4d_{xy}$ become more covalent, while at the same time the negative LF contribution to $g_\parallel$ decreases. This gives rise to $\Delta g_\parallel$

Table 2 Principal Δg values (ppt) and angle α between the principal g_3 and z axis

Fold angle (°)	Δg_1	Δg_2	Δg_3	α (°)
CASPT2 (15in12)				
5.0	−26.7	−71.8	−12.4	55.5
9.0	−24.6	−66.5	−5.4	54.4
13.0	−26.5	−77.2	−3.9	48.1
17.0	−33.3	−87.8	−4.8	46.9
21.0	−37.1	−93.3	−2.0	44.8
25.0	−38.8	−98.3	−0.6	43.8
29.0	−38.8	−98.3	−0.8	43.8
DFT				
21.3 (BP86 [20])	−16.0	−51.5	13.8	
opt (BP86 [50])	−21.2	−68.2	13.4	
21.3 (B3LYP [20])	−23.9	−61.0	9.2	
31.0 (B3LYP [20])	−33.2	−78.1	16.6	
Experiment				
Toluene [10]	−30.0	−68.0	2.0	
Chloroform [14]	−29.3	−66.3	0.2	

values of −114, −75, and +18 ppt for F, Cl, and Br, respectively. The corresponding $\Delta g_\perp$ values of −79, −60, and −59 do not change much in comparison, as they originate only from LF transitions whose energy and covalency are governed by the Mo–O interaction.

The **g** matrix of (Tp*)MoO(bdt) is very similar to that of the $MoOX_4^-$ complexes. The $d_{x^2-y^2} \rightarrow d_{xz,yz}$ LF transitions give rise to negative contributions to $g_{xx,yy}$, while g_{zz} has both a negative contribution from the $d_{x^2-y^2} \rightarrow d_{xy}$ LF transition as well as a positive contribution from the $a''(S_{ip}) \rightarrow d_{x^2-y^2}$ LMCT transition. Consequently, $\Delta g_{xx,yy}$ is controlled by the amount of Mo–O interaction, while Δg_{zz} is governed by the covalency of the in-plane Mo–dithiolate interaction. However, unlike the **g** matrix of the $MoOX_4^-$ complexes, also off-diagonal g_{yz} and g_{zy} contributions appear, arising from the tilted d_{xz} orbital. This means that after diagonalization g_{xx} is unaffected, resulting in a g_1 value along the x axis. On the other hand, g_{yy} and g_{zz} are pushed apart to obtain g_2 and g_3, with the principal axes in the yz plane approximately along the diagonals of the y and z axes. The principal Δg values of (Tp*)MoO(bdt) for each fold angle are summarized in Table 2. The angle between the g_3 and z axis is indicated as α.

When comparing our results to the DFT [20, 50] and experimental [10, 14] values, we can see that near the X-ray fold angle (21.3°) the deviations of the calculated g values with respect to the experimental values have a different sign, i.e. lower for CASPT2 and higher for DFT. The latter deviation is to be expected as DFT tends to overestimate the covalency of polar metal–ligand bonds [20, 51]. Another difference is that in our CASPT2 study, the positive LMCT contribution can be pinpointed to one specific state, i.e. the LMCT transition out of the $a''(S_{ip})$ orbital, whereas with DFT this contribution is distributed over the occupied orbitals resulting in a cumulative effect of a large number of small shifts.

Because the method used here relies on the inclusion of all major contributing excited states, it cannot be excluded that higher lying LMCTs may still provide small contributions. We note however that both with CASPT2 and DFT, g factors obtained near the optimum fold angles (31.0° for DFT, 14.4° for CASPT2) are closer to the experimental values than with the experimental dithiolate fold angle. Other possible reasons for the deviations between the calculated and experimental data are the absence of environment effects in the calculations and the use of a limited basis set. The latter have been shown to significantly influence the calculated g values [52].

4 Conclusion

We have investigated the electronic structure of the ground and first 17 excited states of the (Tp*)MoO(bdt) molecule, as a model for the active site of a range of oxomolybdenum enzymes. At the center of this is the MoO-dithiolate interaction. The dithiolate ligand was found to interact with the molybdenum center through σ bonding interactions between the $a''(S_{ip})$ and $a''(d_{xy})$ orbitals. No evidence was found of a suggested 3-center pseudo-σ bond, believed to probe the coupling into protein mediated superexchange pathways [1]. This was complemented by our alternative assignment of band **4** as the $[a''(S_{ip}) \rightarrow a'(d_{x^2-y^2})]$ instead of the $[a'(S_{ip}) \rightarrow a'(d_{x^2-y^2})]$ LMCT transition.

As expected, the main (negative) contributions to the g values arise from the LF transitions. The g_{xx} and g_{yy} values (along the x axis) are governed by the covalency of the antibonding axial π orbitals, which leads to larger negative g shifts for weaker π-base axial ligands (e.g. sulfur). The g_{zz} value is controlled by the $a''(d_{xy})$ and $a''(S_{ip})$ orbitals, which give a negative and positive contribution, respectively. This leads to larger g values as the covalency of the in-plane Mo–dithiolate σ interaction increases. The principal g_1 value is equal to g_{xx}, while the final g_2 and g_3 values are determined by the initial splitting between g_{yy} and g_{zz} as well as the off-diagonal contributions which are determined by the covalency and orientation of the $a''(d_{xz})\pi$ antibonding orbital. These observations are consistent with the behaviour of previous experimental and calculated g values of a range of (Tp*)MoXL (X = O, S; L = cat, bdt) complexes [14, 20, 50].

The observation that the energy as well as the composition of the excited states doesn't change dramatically over a fold angle range of 5–29° shows that the importance

of the fold angle for (Tp*)MoO(bdt) should not be overestimated. Moreover, the effect of the fold angle on the ground state electronic structure seems to be minimal, as could be expected from the very flat potential energy surface. This is confirmed by the very small variation in g values for the different fold angles of which the main influence is an increased anisotropy of the g_2 and g_3 values with larger angles. As the catalytic cycle of the molybdenum enzymes involves different oxidation states of Mo and as the nature of the dithiolate ligand can vary among the enzymes, further systematic ab initio studies of the electronic structure and influence of the dithiolate fold angle of other models than (Tp*)MoO(bdt) would be of interest.

Acknowledgments This investigation was supported by grants from the Concerted Research Action of the Flemish Government (GOA) and the Flemish Science Foundation (FWO) of which S. V. is a fellow.

References

1. Inscore FE, McNaughton R, Westcott BL, Helton ME, Jones R, Dhawan IK, Enemark JH, Kirk ML (1999) Inorg Chem 38:1401–1410
2. Burgmayer SJN, Kim M, Petit R, Rothkopf A, Kim A, BelHamdounia S, Hou Y, Somogyi A, Habel-Rodriguez D, Williams A, Kirk ML (2007) J Inorg Biochem 101:1601–1616
3. Hille R (1996) Chem Rev 96:2757–2816
4. Garner CD, Banham R, Cooper SJ, Davies ES, Stewart LJ (2001) Enzymes and proteins containing molybdenum or tungsten. In: Bertini I, Sigel A, Sigel H (eds) Handbook on metalloproteins, Ch 22. CRC Press, Boca Raton
5. Westcott BL, Gruhn NE, Enemark JH (1998) J Am Chem Soc 120:3382–3386
6. Helton ME, Kirk ML (1999) Inorg Chem 38:4384–4385
7. Helton ME, Gruhn NE, McNaughton RI, Kirk ML (2000) Inorg Chem 39:2273–2278
8. Carducci MD, Brown C, Solomon EI, Enemark JH (1994) J Am Chem Soc 116:11856–11868
9. Dhawan IK, Pacheco A, Enemark JH (1994) J Am Chem Soc 116:7911–7912
10. Dhawan IK, Enemark JH (1996) Inorg Chem 35:4873–4882
11. Mader ML, Carducci MD, Enemark JH (2000) Inorg Chem 39:525–531
12. Lim BS, Willer MW, Miao M, Holm RH (2001) J Am Chem Soc 123:8343–8349
13. Inscore FE, Joshi HK, McElhaney AE, Enemark JH (2002) Inorg Chim Acta 331:246–256
14. Drew SC, Hill JP, Lane I, Hanson GR, Gable RW, Young CG (2007) Inorg Chem 46:2373–2387
15. McElhaney AE, Inscore FE, Schirlin JT, Enemark JH (2002) Inorg Chim Acta 341:85–90
16. Joshi HK, Cooney JJA, Inscore FE, Gruhn NE, Lichtenberger DL, Enemark JH (2003) Proc Natl Acad Sci 100:3719–3724
17. Joshi HK, Enemark JH (2004) J Am Chem Soc 126:11784–11785
18. Cooney JJA, Cranswick MA, Gruhn NE, Joshi HK, Enemark JH (2004) Inorg Chem 43:8110–8118
19. Domercq B, Coulon C, Fourmigue M (2001) Inorg Chem 40:371
20. Drew SC, Young CG, Hanson GR (2007) Inorg Chem 46:2388–2397
21. Pierloot K (2005) Calculation of electronic spectra of transition metal complexes. In: Olivucci M (ed) Computational photochemistry, vol 16. Elsevier, Amsterdam
22. Ahlrichs R, Bar M, Häser M, Horn H, Kolmel C (1989) Chem Phys Lett 162:165–169
23. Dirac PAM (1929) Proc R Soc London A 123:714–733
24. Slater JC (1951) Phys Rev 81:385–390
25. Perdew JP, Wang, Y (1996) Phys Rev B 45:13244–13249
26. Perdew JP, Burke K, Ernzerhof M (1996) Phys Rev Lett 77:3865–3868
27. Perdew JP, Ernzerhof M, Burke K (1996) J Chem Phys 105:9982–9985
28. Schäfer A, Huber C, Ahlrichs R (1994) J Chem Phys 100:5829
29. Eichkorn K, Weigend F, Treutler O, Ahlrichs R (1997) Theor Chem Acc 97:119
30. Malmqvist P-Å, Rendell A, Roos BO (1990) J Phys Chem 94:5477–5482
31. Andersson K, Malmqvist P-Å, Roos BO, Sadlej AJ, Wolinski K (1990) J Phys Chem 94:5483–5488
32. Andersson K, Malmqvist P-Å, Roos BO (1992) J Chem Phys 96:1218–1226
33. Karlström G, Lindh R, Malmqvist P-Å, Roos BO, Ryde U, Veryazov V, Widmark P-O, Cossi M, Schimmelpfennig B, Neograd y P, Seijo L (2003) Comput Mater Sci 28:222–239
34. Douglas M, Kroll NM (1974) Ann Phys 82:89–115
35. Hess BA (1986) Phys Rev A 33:3742–3748
36. Wolf A, Reiher M, Hess BA (2002) J Chem Phys 117:9215–9226
37. Forsberg N, Malmqvist P-Å (1997) Chem Phys Lett 274:196–204
38. Ghigo G, Roos BO, Malmqvist P-Å (2004) Chem Phys Lett 396:142–149
39. Aquilante F, Malmqvist P-Å, Pedersen TB, Ghosh A, Roos BO (2008) J Chem Theor Comp 4:694
40. Pierloot K (2003) Mol Phys 101:2083
41. Pierloot K (2000) Nondynamic correlation effects in transition metal coordination compounds. In: Cundari TR (ed) Computational organometallic chemistry. Marcel Dekker, New York
42. Malmqvist P-Å, Roos BO (1989) Chem Phys Lett 155:189–194
43. Neese F (2004) Magn Reson Chem 42:S187–S198
44. Vancoillie S, Malmqvist P-Å, Pierloot K (2007) Chem Phys Chem 8:1803–1815
45. Bolvin H (2006) Chem Phys Chem 7:1575–1589
46. Finley J, Malmqvist P-Å, Roos B, Serrano-Andrés L (1998) Chem Phys Lett 288:299–306
47. Hess BA, Marian CM, Wahlgren U, Gropen O (1996) Chem Phys Lett 251:365–371
48. Christiansen O, Gauss J, Schimmelpfennig B (2000) Phys Chem Chem Phys 2:965–971
49. Vahtras O, Engström M, Schimmelpfennig B (2002) Chem Phys Lett 351:424–430
50. Fritscher J, Hrobárick P, Kaupp M (2007) Inorg Chem 46:8146–8161
51. Neese F (2001) J Phys Chem A 105:4290
52. Vancoillie S, Pierloot K (2008) J Phys Chem A 112:4011–4019